Winter 1-18-2012

Convection in Stable and Unstable Fronts

Desiderio A. Vasquez
vasquez@ipfw.edu

Drew Elliot

This research is a product of the Department of Physics faculty at Indiana University-Purdue University Fort Wayne.

Convection in stable and unstable fronts

Drew Elliott[1] and Desiderio A. Vasquez[1,2,*]

[1]*Department of Physics, Indiana University Purdue University Fort Wayne, Fort Wayne, Indiana 46805, USA*
[2]*Departamento de Ciencias, Sección Física, Pontificia Universidad Católica del Perú, Avenida Universitaria 1801, San Miguel, Lima 32, Peru*

Density gradients across a reaction front can lead to convective fluid motion. Stable fronts require a heavier fluid on top of a lighter one to generate convective fluid motion. On the other hand, unstable fronts can be stabilized with an opposing density gradient, where the lighter fluid is on top. In this case, we can have a stable flat front without convection or a steady convective front of a given wavelength near the onset of convection. The fronts are described with the Kuramoto-Sivashinsky equation coupled to hydrodynamics governed by Darcy's law. We obtain a dispersion relation between growth rates and perturbation wave numbers in the presence of a density discontinuity acccross the front. We also analyze the effects of this density change in the transition to chaos.

I. INTRODUCTION

The Rayleigh-Taylor instability, caused by a heavier fluid placed on top of a lighter one, appears in a wide variety of physical systems, such as laser ablation [1,2], astrophysics [3], liquid-gas interfaces [4], combustion [5,6], and chemical reaction fronts [7,8]. The fluids involved are usually separated by an interface that contains a stabilizing mechanism, such as surface tension [9] or molecular diffusivity (as in the case of a chemical front) [10]. In other cases, the front itself is unstable regardless of fluid motion, caused either by differences in molecular diffusivities [11] or by a combination of diffusion and heat as in the case of combustion [12]. This front instability can be modeled using coupled reaction-diffusion equations or a heat equation coupled to a diffusion equation, with no need for hydrodynamic equations. The propagation of these fronts can be approximated with a Kuramoto-Sivashinsky (KS) equation, which provides conditions for instabilities of flat fronts and determines the front evolution in the weakly nonlinear regime [13,14]. Under certain conditions, the KS equation exhibits instability of flat fronts for perturbations of wavelengths greater than a critical wavelength. This implies that fronts propagating in narrow tubes will be flat. Increasing the width of the tube allows the formation of steady cellular structures, however, these cells are limited to only a very few wavelengths. For even larger tube widths the cell structures become oscillatory and, finally, chaotic [15]. A common mechanism for obtaining structures of several wavelengths is to add a linear stabilizing term, usually justified on phenomenological grounds [16,17]. The presence of this linear term allows steady cellular structures of many wavelengths. This wavelength is selected intrinsically by the equation parameters, regardless of the domain size. In this paper we investigate the interaction between Rayleigh-Taylor instabilities and front instabilities described by KS equations. Every system with the lighter fluid on top is stable with respect to the Rayleigh-Taylor mechanism. We show that this mechanism coupled to an unstable front will form a steady pattern with an intrinsic wavelength.

II. EQUATIONS OF MOTION

Our work focuses on two fluids of different densities separated by a thin interface. We study the case of two-dimensional flow in porous media or a Hele-Shaw cell. The front separating the fluids is described by the front height $H(X,T)$, which provides the vertical Z coordinate as a function of the horizontal coordinate X, and the time T. The external fluid velocity adds to the front speed as discused by Spangler and Edwards in the context of the eikonal relation [18]. In the same manner, the front propagation will obey the KS equation with the addition of fluid flow:

$$\frac{\partial H}{\partial T} = V_0 + \nu \frac{\partial^2 H}{\partial X^2} + \frac{V_0}{2}\left(\frac{\partial H}{\partial X}\right)^2 - \kappa \frac{\partial^4 H}{\partial X^4} + V_z\bigg|_H. \quad (1)$$

Here V_0 corresponds to the flat front speed, while V_z corresponds to the vertical component of the fluid velocity, which is evaluated at the front height H. The coefficients ν and κ depend on the details of the system under consideration under a particular set of units. For example, in the case of thermodiffusive instabilities, they depend on the Lewis number, which is the ratio of thermal diffusivity and mass diffusivity [14]. For the case of autocatalytic reaction fronts, the normal front velocity can be obtained from an eikonal relation between the molecular diffusivity (D) and the front curvature, leading to $\nu = D$ and $\kappa = 0$ for small curvatures. For autocatalytic fronts involving two species, the coefficients ν and κ will depend on the ratio between their different diffusivities [13].

In this paper, we use Darcy's law to describe fluid flow in porous media or a Hele-Shaw cell,

$$\vec{V} = -\frac{K}{\mu}(\vec{\nabla}P + \rho g \hat{e}_z), \quad (2)$$

together with the continuity equation,

$$\vec{\nabla} \cdot \vec{V} = 0. \quad (3)$$

Here $\vec{V}$ is the fluid velocity, P is the pressure, g is the acceleration of gravity in the vertical direction, $\hat{e}_z$ is a unit vector in the vertical direction pointing upward, K is the coefficient of permeability, and μ is the coefficient of viscosity. In a Hele-Shaw cell, where a viscous fluid is confined between

_____
*vasquez@ipfw.edu

two walls separated by a small distance a, the coefficient of permeability can be replaced by $a^2/12$. In the thin front approximation, there is an abrupt change of density across the front that can be written as

$$\rho = \rho_0 + \Delta\rho\Theta(Z - H), \tag{4}$$

where Θ is the a step function, being equal to 1 if the argument is positive and 0 otherwise. The density difference between unreacted and reacted fluid corresponds to $\Delta\rho$; it will be positive if the heavier fluid is on top. The continuity equation allows us to write the components of the fluid velocity in terms of a stream function $\Psi(X,Z,T)$ using $V_x = -\partial\Psi/\partial Z$ and $V_z = \partial\Psi/\partial X$. Introducing these relations into Darcy's law and combining them to eliminate the pressure, we find an equation for the stream function:

$$\nabla^2\Psi = \tilde{R}\frac{\partial H}{\partial X}\delta(Z - H(X,T)). \tag{5}$$

Here we have defined $\tilde{R} = Kg\Delta\rho/\mu$. The Dirac δ function $\delta(z)$ results from the derivative of the step function, having as units the inverse of length units. This equation provides the stream function (and therefore the fluid velocity) for a given value of H. Consequently, the front evolution [Eq. (1)] is governed only by the front height H. Assuming that κ is nonzero, we introduce time and length scales defined by $L_T = \kappa/v^2$, $L_x = \sqrt{(\kappa/|v|)}$, and $L_z = |v|/V_0$. The stream function is measured in units of $L_x L_z/L_T$. Using lowercase letters for the corresponding variable in this system of units, the equations of motion become

$$\frac{\partial h}{\partial t} = c_0 + \tilde{v}\frac{\partial^2 h}{\partial x^2} + \frac{1}{2}\left(\frac{\partial h}{\partial x}\right)^2 - \frac{\partial^4 h}{\partial x^4} + \frac{\partial\psi}{\partial x}\Big|_h \tag{6}$$

and

$$\frac{\partial^2\psi}{\partial x^2} + \beta^2\frac{\partial^2\psi}{\partial z^2} = \beta Ra\frac{\partial h}{\partial x}\delta(z - h(x,t)). \tag{7}$$

Here we have defined the dimensionless numbers $Ra = \tilde{R}L_x/v$, $\beta = L_x/L_z$, and $c_0 = V_0^2\kappa/|v|^3$. The value of $\tilde{v}$ is either $+1$ or -1, depending on the original sign of v; therefore, we have $\tilde{v} = v/|v|$.

We solve this equation by introducing Fourier series on h and ψ:

$$\psi = \sum_{n=1}\psi_n(z,t)\sin(nqx) \tag{8}$$

and

$$h = \sum_{n=0}H_n(t)\cos(nqx). \tag{9}$$

Here the parameter q is determined by the width of the domain (a): $q = \pi/a$. The x coordinate varies from 0 to a. Each Fourier series corresponds to the appropriate boundary conditions at the vertical walls: horizontal fluid velocity 0 $(v_x = 0)$ and 0 first and third derivatives for the front height $(\partial h/\partial x = \partial h^3/\partial x^3 = 0)$ [19]. We keep only a linear dependence between the stream function and the front height measured from the average front height. The Fourier coefficient $H_0(t)$ provides the average front height. This results in evaluation of the derivative of the stream function in Eq. (6) on H_0 instead of h and replacement of h with H_0 inside the δ

function in Eq. (7). In this approximation the stream function ψ remains continuous across the front, while the δ function in Eq. (7) leads to a jump condition for the partial derivative of the stream function along the z direction:

$$\lim_{\epsilon\to 0}\beta^2\left[\frac{\partial\psi}{\partial z}\Big|_{z=H_0+\epsilon} - \frac{\partial\psi}{\partial z}\Big|_{z=H_0-\epsilon}\right] = \beta Ra\frac{\partial H}{\partial x}. \tag{10}$$

We find that the Fourier components of the stream function are given by

$$\psi_n(z,t) = \begin{cases} (RaH_n/2)e^{-nq(z-H_0)/\beta} & \text{if } z > H_0, \\ (RaH_n/2)e^{nq(z-H_0)/\beta} & \text{if } z \leqslant H_0. \end{cases} \tag{11}$$

Using this expression to evaluate the vertical component of the velocity at the front, we find

$$\frac{\partial h}{\partial t} = c_0 + \tilde{v}\frac{\partial^2 h}{\partial x^2} + \frac{1}{2}\left(\frac{\partial h}{\partial x}\right)^2 - \frac{\partial^4 h}{\partial x^4} + \frac{Ra}{2}\sum_n(nq)H_n\cos(nqx). \tag{12}$$

Introducing the Fourier series for $h(x,t)$ and projecting over the corresponding cosine function, we obtain a set of ordinary differential equations:

$$\frac{dH_0}{dt} = c_0 + \frac{q^2}{4}\sum_p p^2 H_p^2, \tag{13}$$

$$\frac{dH_n}{dt} = \left[-\tilde{v}(nq)^2 - (nq)^4 + Ra\frac{nq}{2}\right]H_n + \frac{q^2}{4}\sum_{l,p}lpH_pH_l$$
$$\times(\delta_{n,|l-p|} - \delta_{n,l+p}) \quad\text{for}\quad n \geqslant 1. \tag{14}$$

This set of equations is solved numerically using a 25 term truncation. We found no significant differences in the steady states with slightly fewer terms. We use a simple Euler method to carry out the time evolution of the equations. The time step is set to $\Delta t = 0.001$ time unit. We initialize our calculations using small random initial conditions for each Fourier coefficient h_n. We let the system evolve for a time in order to eliminate transient behavior. The spatial front is reconstructed from the Fourier amplitudes [Eq. (9)] using a spatial grid of 100 points.

III. RESULTS

We carry out a linear stability analysis of the flat front solution by neglecting the quadratic terms in Eq. (12). We truncate the Fourier expansion to one term while looking for solutions of the form $he^{\sigma t}$. We find a dispersion relation between the growth rate σ and the wave number q given by

$$\sigma = -\tilde{v}q^2 - q^4 + q Ra/2. \tag{15}$$

The dispersion relation does not depend on the flat front speed v_0, since it only appears in the quadratic terms. The front will be stable for all values of the wave number where σ is negative. We note that the growth rate σ vanishes for $q = 0$, which is a consequence of translational invariance. The stability of the front will depend on two parameters, $\tilde{v}$ and Ra. We first analyze the case where $\tilde{v} = 1$. For no density differences or when the lighter fluid is on top ($Ra \leqslant 0$), the

front is stable for all values of q. Instability can be achieved only when the heavier fluid is on top (Ra > 0) For small values of q, the dispersion relation will be proportional to Ra ($\sigma \approx q\text{Ra}/2$), therefore for long-wavelength perturbations (q small), the stability will be determined by the sign of Ra. For short-wavelength perturbations (q large), the value of σ will always be negative since in this range $\sigma \approx -q^4$, regardless of the value of Ra. Since Ra positive makes the front unstable for small values of q, but stable for large q, there is a critical wave number for marginal stability (where $\sigma = 0$). This implies that if the front propagates in tubes of width smaller than the corresponding critical wavelength, the front will be stable, since the tube width will provide a cutoff for the allowed wave numbers. The relation between this critical wave number and the tube width is provided by $q_c = \pi/L_c$. For small values of Ra we can obtain the critical wave number by neglecting the q^4 term in the dispersion relation. This approximation results in a critical width given by $L_c = 2\pi/\text{Ra}$. This is the same result obtained for autocatalytic fronts described by the eikonal relation between front speed and curvature [20]. In Fig. 1 we compare this approximation for the critical width with the full result using the KS equations. The figure shows good agreement for small values of Ra, but they become different as this number increases. Figure 1 also shows the stabilizing effect of the fourth-order derivative in the front evolution equation.

In the case of $\tilde{v} = -1$, the front presents an instability even without a density difference. With Ra $= 0$ the front propagation equation becomes the standard KS equation, which is unstable for perturbations of wave number smaller than $q = 1$ (Fig. 2). This instability has been widely study in the literature. The dispersion relation of the standard KS equation is dominated by the positive q^2 term for short wave numbers. Therefore the front will always be unstable for these perturbations. But for large wave numbers, the dispersion relation is dominated by the negative q^4 term, indicating stability for these values. However, including fluid flow driven
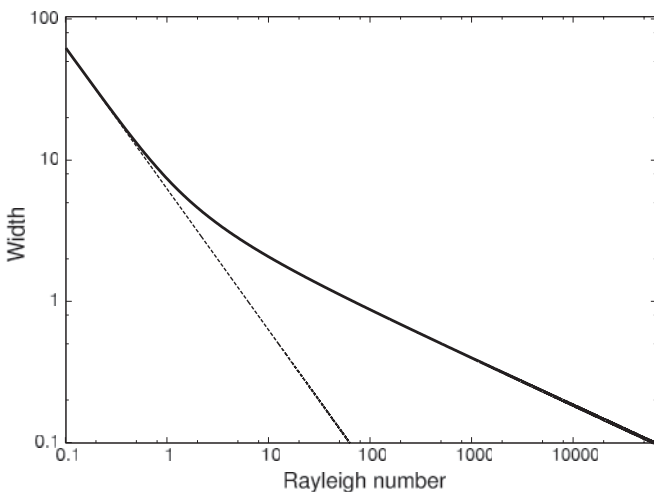

FIG. 2. Growth rate (σ) as a function of wave number q for different values of the Rayleigh number for $\tilde{v} = -1$. The solid line corresponds to Ra $= 0$, showing unstable perturbations even without a density difference. The bold line at the top corresponds to Ra $= 1$. The dashed line corresponds to Ra $= -4\sqrt{3}/9$, with its maximum equal to 0 at $q = 1/\sqrt{3}$. The dotted line corresponds to Ra $= -1$. Units are the dimensionless units described in the text.

by a density gradient, we find that the short wave-number limit becomes proportional to the wave number q multiplied by Ra. For Ra > 0, the Rayleigh-Taylor instability will contribute to making the front more unstable, but short wavelengths will still be dominated by the negative q^4 term in the dispersion relation, therefore a stable flat front can always be found by choosing the necessary domain width. For Ra < 0 we find that the growth rate σ will be negative for both large q and very small q. However, for Ra $>$ R$_m \equiv -4\sqrt{3}/9$ there is an interval where the growth rate is positive, indicating that certain perturbations

FIG. 1. Critical width as a function of Rayleigh number. The solid line corresponds to fronts described by a stable Kuramoto-Sivashinsky equation ($\tilde{v} = 1$). The dotted line corresponds to fronts described by the eikonal relation, which provides the stabilizing mechanism.
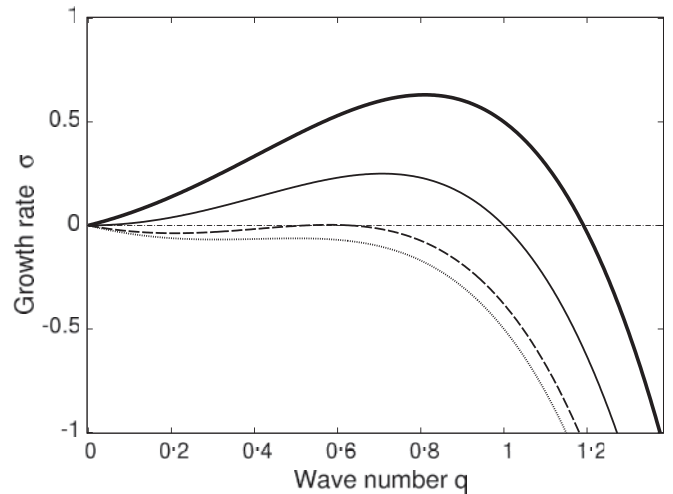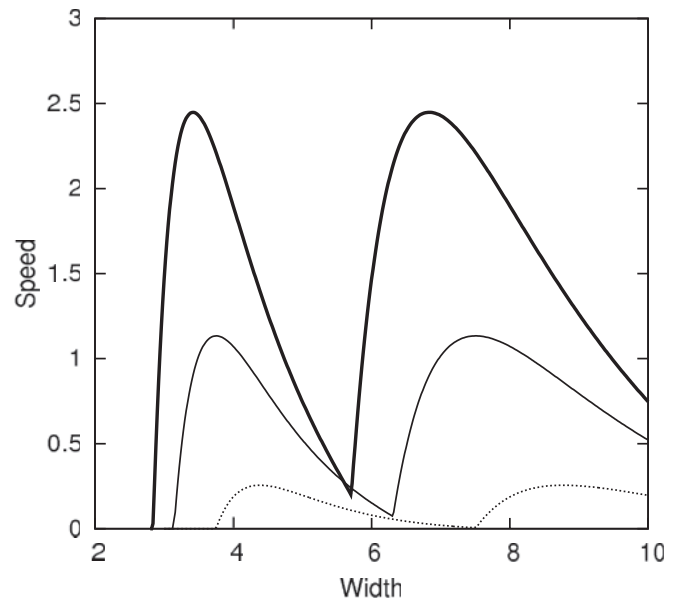

FIG. 3. Increase in speed as a function of domain width for different values of the Raleigh number ($\tilde{v} = -1$). The bold line corresponds to Ra $= 0.5$, the solid line corresponds to Ra $= 0$, and the dotted line corresponds to Ra $= -0.5$.
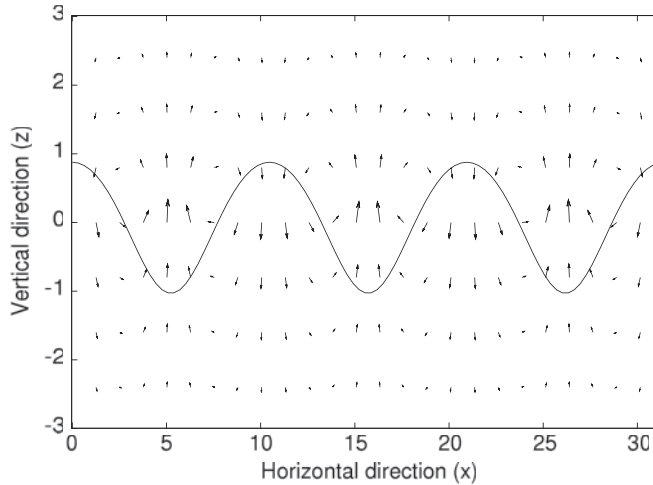
FIG. 4. Fluid velocity near a steady convective front. Here Ra = −0.65. The lighter fluid is above the front. Without fluid motion the front would be unstable since $\tilde{v} = -1$.
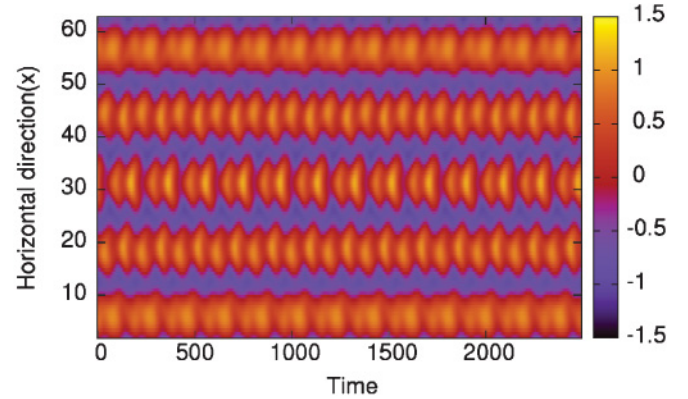

FIG. 5. (Color online) Time evolution of an oscillatory front. Colors (gray scale) represent different front heights measured relative to the average front position. The width of the rectangular domain corresponds to 20π; the Rayleigh number is Ra = −0.65 ($\tilde{v} = -1$).

will make the front unstable. This feature is not present in the standard KS equation. At Ra = R_m we find that the curve touches the horizontal axis ($\sigma = 0$) at exactly one point with $q = 1/\sqrt{3}$ as shown in Fig. 2

We solve the nonlinear equations Eqs. (12) and (13) numerically as described in Sec. II. We first study the effects of the density differences on the confined patterns. As the linear stability analysis suggests, the front is flat and stable for small widths, becoming unstable for widths above a critical value. Near the transition, small perturbations on an unstable flat front grow until they reach a steady state. The resulting curved front propagates at a constant speed. In Fig. 3 we display the increase in front speed as a function of tube width for three values of Ra. For fronts without a density gradient (Ra = 0), we find that slightly above the critical width $L_c = \pi$, the front becomes a steady curved front without a definite symmetry. The front speed increases until it reaches a maximum, then it decreases. As the width is further increased, the front becomes axisymmetric, with its maximum height at the center of the tube. The front speed will increase once again, reaching a second maximum, and then decreasing. The same behavior can be found with negative and positive values of Ra. As we increase the width of the tube, the steady front changes from flat, to nonaxisymmetric, to axisymmetric. However, the points where the transitions take place are shifted. When the lighter fluid is on top of the heavier fluid (Ra < 0), buoyancy provides a stabilizing mechanism, consequently the transitions take place at larger widths. On the contrary, if the heavier fluid is on top, the destabilizing effect of buoyancy will allow the transitions to occur at lower widths. Buoyancy also plays a role in the front speed: the increase in speed is higher when the lighter fluid is below the heavier fluid.

We also study the spatiotemporal behavior near Ra = R_m, where the instability takes place at a definite wavelength. For values of Ra below this critical value, all the growth rates are negative, therefore no pattern is formed. At Ra = −0.675, we found that small perturbations to the flat front grow, generating the pattern shown in Fig. 4. The pattern moves at a constant speed along the tube without distortion; it is

steady in a reference frame comoving with the front. Although we display the pattern on a domain size $L = 10\pi$, its shape is not determined by the size of the domain. In larger domains we also found an extended steady pattern with almost the same wavelength. The wavelength of the pattern is determined intrinsically. We also display in Fig. 4 the corresponding fluid flow associated with the stationary front. Here we find that in the valleys, the fluid tends to rise, while in the crest, the fluid pushes downward. This is the result of having the heavier fluid underneath: heavier fluid will try to fill up the gaps. Without this convective flow, the reaction front will be unstable, behaving in a chaotic manner. The front instability combined with the stabilizing density gradient leads to a steady structure. As we keep increasing the value of Ra, the front develops a temporal behavior. In Fig. 5 we show the time evolution of the reaction front with Ra = −0.65. Here we observe a complex oscillatory pattern where the pattern repeats itself after a number of fluctuations. For Ra = −0.625 the pattern becomes chaotic as shown in Fig. 6.

We also find a period doubling transition to chaos as we change the width of the domain (L), which is equivalent to
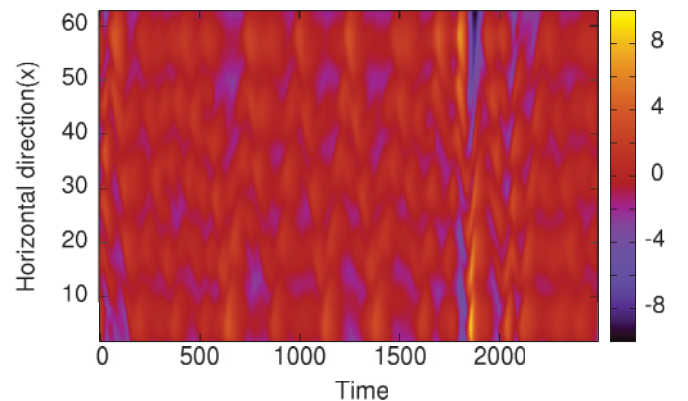

FIG. 6. (Color online) Time evolution of a chaotic front. Colors (gray scale) represent different front heights measured relative to the average front position. The width of the rectangular domain corresponds to 20π; the Rayleigh number is Ra = −0.625 ($\tilde{v} = -1$).
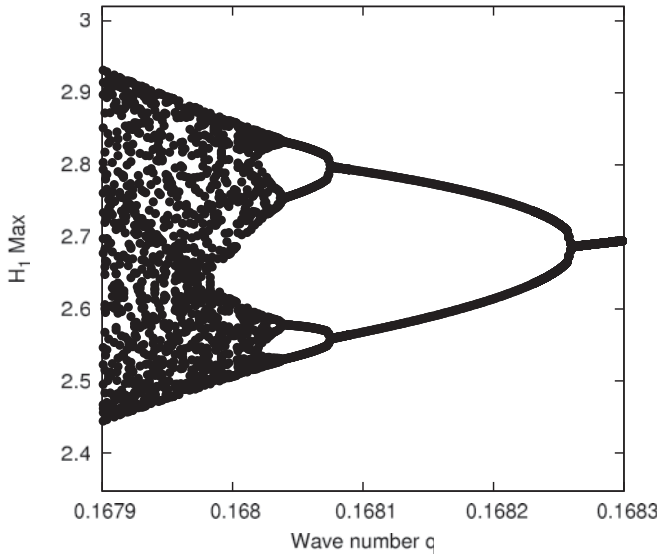
FIG. 7. Bifurcation diagram showing relative maxima on the time evolution for the Fourier mode amplitude H_1. Here we observe period-doubling bifurcations as we reduce the control parameter q. The Rayleigh number is Ra = 0.1.

changing the parameter $q = \pi/L$. This transition is similar to the one observed by Horváth *et al.* [11] in a system without fluid motion. Without fluid motion (Ra = 0) we obtain a transition from a steady pattern to an oscillatory pattern at $q = 0.1885$. For nonzero Rayleigh numbers the transition is shifted to a different value of q. For Ra = 0.1 the transition takes place at $q = 0.1924$, while for Ra = −0.1 we find this transition at $q = 0.1822$. This is consistent with the fact that a negative Ra provides stability to the front by having the lighter fluid on top. A more stable front requires a wider tube
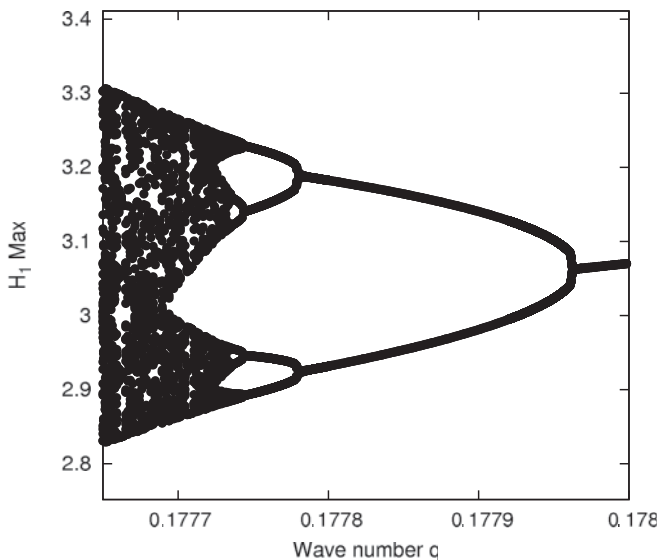

FIG. 8. Bifurcation diagram showing relative maxima on the time evolution for the Fourier mode amplitude H_1. Here we observe period-doubling bifurcations as we reduce the control parameter q. The Rayleigh number is Ra = −0.1.

width (smaller q) to trigger the instability. In Fig. 7 we show the period-doubling bifurcations that lead to chaos in systems with positive and negative Ra values. Here we display the relative maximum values of the first Fourier coefficient H_1 as it varies with time. The transition to chaos takes place as we decrease q. In the graph with Ra = 0.1 we find an oscillatory behavior at $q = 0.1780$. This is represented in the graph by a single point corresponding to a single relative maximum value for H_1. As we decrease q, we find a period-doubling bifurcation at $q = 0.17796$. These bifurcations continue for decreasing q, leading to a chaotic regime. We obtain a similar period-doubling transition for Ra = −0.1, however, the first transition occurs at a lower value of q, namely, $q = 0.16827$ as shown in Fig. 8. Therefore a density gradient with the lighter fluid on top also tends to suppress the oscillatory instabilities, since a lower value of q corresponds to a larger width for the transition.

IV. SUMMARY AND DISCUSSION

We have shown that density gradients across a thin front can play a significant role in the propagation of fronts governed by the KS equation. These density gradients can lead to convection for fronts propagating in fluids. It can destabilize fronts that are stable without fluid motion or it can stabilize potentially unstable fronts. The KS equation does not exhibit stable patterns at many wavelengths, unless a linear stabilizing term is included. We have shown that a density gradient across the front can also provide a necessary stabilizing mechanism for this type of structure. The KS equation has long been studied because it exhibits spatiotemporal chaos. In the presence of density gradients this transition to chaos is affected. When the lighter fluid is above, the onset of chaos is delayed to larger values of the control parameter (the tube width in this case). The flat front instability leading to convection depends only on the dimensionless Rayleigh number Ra; this number does not depend on the front velocity. Therefore, the instability for fronts propagating upward is the same as for fronts propagating downward, depending only on the density gradient and other parameters. Experiments can test the gravitational effects by reversing the direction for the vertical front propagation. Using typical values for the iodate–arsenous acid reaction, we obtain a dimensionless Rayleigh number of between 50 and 60 on a Hele-Shaw cell with a 1-mm gap. This value is still large compared to the value of 0.769, which allows the formation of extended periodic structures. The search for these structures will require lowering the Rayleigh number by reducing the gap width or using only a small angular deviation from the horizontal position as suggested in [21]. The typical dimensionless wave number of these patterns is $q = 1/\sqrt{3}$, which corresponds to a dimensioned wavelength of 1.6 mm for this system.

[1] S. E. Bodner, Phys. Rev. Lett. **33**, 761 (1974).

[2] H. Azechi, T. Sakaiya, S. Fujioka, Y. Tamari, K. Otani, K. Shigemori, M. Nakai, H. Shiraga, N. Miyanaga, and K. Mima, Phys. Rev. Lett. **98**, 045002 (2007).

[3] L. Smarr, J. R. Wilson, R. T. Barton, and R. L. Bowers, Astrophys. J. **246**, 515 (1981).

[4] G. H. Wolf, Phys. Rev. Lett. **24**, 444 (1970).

[5] N. Vladimirova and R. Rosner, Phys. Rev. E **67**, 066305 (2003).

[6] Z. Rakib and G. I. Sivashinsky, Combust. Sci. Technol. **54**, 69 (1987).

[7] J. D'Hernoncourt, A. Zebib, and A. DeWit, Phys. Rev. Lett. **96**, 154501 (2006).

[8] J. Masere, D. A. Vasquez, B. F. Edwards, J. W. Wilder, and K. Showalter, J. Phys. Chem. **98**, 6505 (1994).

[9] D. H. Sharp, Physica D **12**, 45 (1984).

[10] D. A. Vasquez, J. M. Littley, J. W. Wilder, and B. F. Edwards, Phys. Rev. E **50**, 280 (1994).

[11] D. Horváth, V. Petrov, S. K. Scott, and K. Showalter, J. Chem. Phys. **98**, 6332 (1993).

[12] G. I. Sivashinsky, Annu. Rev. Fluid Mech. **15**, 179 (1983).

[13] A. Malevanets, A. Careta, and R. Kapral, Phys. Rev. E **52**, 4724 (1995).

[14] G. I. Sivashinsky, Acta Astronaut. **4**, 1177 (1977).

[15] I. G. Kevrekidis, B. Nicolaenko, and J. C. Scovel, SIAM. J. Appl. Math. **50**, 760 (1990).

[16] C. Misbah and A. Valance, Phys. Rev. E **49**, 166 (1994).

[17] D. Obeid, J. M. Kosterlitz, and B. Sandstede, Phys. Rev. E **81**, 066205 (2010).

[18] R. S. Spangler and B. F. Edwards, J. Phys. Chem. **118**, 5911 (2003).

[19] S. B. Margolis and G. I. Sivashinsky, SIAM J. Appl. Math. **44**, 344.

[20] D. A. Vasquez, J. W. Wilder, and B. F. Edwards, J. Chem. Phys. **104**, 9926 (1996).

[21] J. D'Hernoncourt, J. H. Merkin, and A. De Wit, J. Chem. Phys. **130**, 114503 (2009).